Prediction and Optimization of Surface-Enhanced Raman Scattering Geometries using COMSOL Multiphysics

I. Knorr[1], K. Christou*[,2], J. Meinertz[1], A. Selle[1], J. Ihlemann[1] and G. Marowsky[1]
[1]Laser-Laboratorium Göttingen e.V.
*Corresponding author: inga.knorr@llg-ev.de

Laser-Laboratorium Göttingen e.V., Hans-Adolf-Krebs-Weg 1, 37077 Gttingen, Germany

Abstract: Raman spectroscopy is a commonly used tool in bio-diagnostics and sensor technology. Surface-enhanced Raman scattering provides high signal enhancements especially at nanostructured metallic surfaces. In this paper the electromagnetic Raman enhancement from different metallic nanostructures – including gold coated gratings, spherical and hemispherical particles – is calculated by using the finite-element method. The characteristic dimensions of the nanostructures are varied and the results are discussed and compared to each other. It is shown that hemispherical particles on a substrate promise the largest enhancement factors of up to seven orders of magnitude. These results are consistent with Raman spectroscopic measurements on surfaces covered with spherical gold particles.

Keywords: Surface-enhanced Raman-scattering (SERS), electromagnetic modelling, plasmons, gold nanostructures.

1 Introduction

Raman scattering is an inelastic scattering process between a photon and a molecule. The scattered photon is shifted in frequency by the energy of the molecule‘s characteristic molecular vibrations. The spectral information of the Raman scattered light enables the identification of the scattering molecules. Therefore Raman spectroscopy is a commonly used tool in bio-diagnostics and sensor technology. However, the Raman scattering cross section is very small (typically $\sigma = 10^{-30}\mathrm{cm}^2$/molecule) which yields low signal strength. Therefore, much effort is made in the field of Surface-Enhanced Raman-scattering (SERS) to increase signal strength and measurement sensitivity. The effect underlying SERS is still not fully understood, and the importance of different influencing factors is a topic of discussion.

It is believed that three major mechanisms are responsible for SERS [3][4]: electromagnetic enhancement arising from high local electromagnetic fields in the proximity of metallic nanostructures induced by plasmon resonance [6], chemical enhancement due to binding of the Raman molecules to the substrate resulting in an increased scattering cross section[1][5] and geometrical enhancement in consequence of an increased surface area. While the chemical enhancement factors are of the order of 100[5], the electromagnetic enhancement can exceed values of 10^6-10^{12} and is therefore the major contributing mechanism for SERS [3].

To account for high electromagnetic enhancement the SERS-surfaces should fulfill three requirements. Firstly, the use of metallic structures, preferably gold or silver because of their plasmon resonance in the visible range and their biocompatibility, is crucial to provide extraordinarily high electromagnetic fields. Secondly, sharp features and strong curvature regions give the largest enhancement because of the lightning rod effect resulting in additionally increased fields. Furthermore, closely spaced interacting particles can provide extra field enhancement in their interstices.

For quantitative methods such as concentration measurements it is necessary that the enhancement factor is constant across the substrate. Periodically structured surfaces offer this feature and have therefore become preferably used geometries for SERS applications.

In order to gain a deeper understanding

of the electromagnetic enhancement effect, COMSOL Multiphysics is used to simulate the electromagnetic fields at nanostructured metallic surfaces and to calculate the SERS enhancement factors. The simulations are carried out in two dimensions and cover gold coated rectangular gratings with varying period and depth as well as spherical and hemispherical gold particles on a fused silica substrate with varying diameter and separation. The reduction of spherical and hemispherical particles to two dimensions can be considered as a section through three-dimensional particles along the line of their centers. The chosen feature sizes and separations are similar for all geometries so that the results may be compared.

2 Experimental

The model is set up in the Scattered Harmonic Propagation Application Mode with periodic boundary conditions (Floquet periodicity) to simulate a unit cell of the periodically structured surface. An incident wave is introduced propagating perpendicular to the surface. As plasmons can only be excited when the E-field is in the plane of incidence, TM-polarized light is considered. The incident plane wave satisfies the relationship

$$\mathbf{E}_i(\mathbf{r},t) = \mathbf{E}_0\, e^{i\mathbf{k}\,\mathbf{r}-i\omega\,t} \tag{1}$$

$$\mathbf{H}_i(\mathbf{r},t) = \mathbf{H}_0\, e^{i\mathbf{k}\,\mathbf{r}-i\omega\,t} \tag{2}$$

where the wave vector is parallel to the y-axis $\mathbf{k} = -k\,\hat{\mathbf{y}}$, the electric field lies in the plane of incidence, which is considered to be the xy-plane, with $\mathbf{E}_0 = E_0\,\hat{\mathbf{x}}$ and the magnetic field is perpendicular to the plane of incidence $\mathbf{H}_0 = H_0\,\hat{\mathbf{z}}$.

As the simulated structures are periodic in one direction, periodic boundary conditions are introduced in x-direction. Perfectly Matched Layers (PML) are used to terminate the computational domain in z-direction. These PMLs match the optical index at the interface and attenuate travelling waves exponentially to prevent unphysically backreflected waves from the outer boundaries.

As geometries different periodic gold nanostructures, including rectangular gratings, spherical and hemispherical particles with varying feature size and separation are simulated.

The simulations cover wavelengths of 450-850nm in order to identify plasmonic resonances and their dependence on geometry parameters. For simplicity, the refractive index of the underlying fused silica substrate is $n = 1.46$ and is assumed to be independent of the illumination wavelength. The optical constants for gold, however, are highly dispersive in the visible range. They are taken from the experimental data of Johnson and Christy [2].

The Raman enhancement originates from locally enhanced electromagnetic fields at the surface of the metallic structures. The Stokes Raman signal is proportional to the square of the local intensity of the electromagnetic field, the surface area and the Raman scattering cross section. The number of Stokes photons per second can be written as [1]

$$P^{\mathrm{SERS}} = \sigma_{ads}^{S}\frac{A}{A_0}\frac{|\mathbf{E}_{loc}(\omega_i)|^2}{|\mathbf{E}_0(\omega_i)|^2}\,\frac{|\mathbf{E}_{loc}(\omega_R)|^2}{|\mathbf{E}_0(\omega_R)|^2} \tag{3}$$

Here, σ_{ads}^{S} is the Stokes-Raman cross section of the adsorbed molecule, A/A_0 is the ratio of the area of the structured surface to the area of an unstructured surface and $|\mathbf{E}_{loc}(\omega)|^2/|\mathbf{E}_0(\omega)|^2\,|\mathbf{E}_{loc}(\omega_R)|^2/|\mathbf{E}_0(\omega_R)|^2$ describes the electromagnetic enhancement factor. This electromagnetic enhancement factor results from the enhancement of the Raman radiation in a two-step-process: Firstly, the excitation of Raman-active molecules is proportional to the square of the local electric field $|\mathbf{E}_{loc}(\omega_i)|^2/|\mathbf{E}_0(\omega_i)|^2$ at the incident frequency which can be very high at the surface of metallic structures. In the second step, the emitted Raman radiation is enhanced by the metal particle resonance which is proportional to the local electric fields at the frequency of the Raman light $|\mathbf{E}_{loc}(\omega_R)|^2/|\mathbf{E}_0(\omega_R)|^2$. In most cases, the frequency of the Raman scattered light is close to that of the incident radiation so that the electromagnetic enhancement factor can be expressed as $|\mathbf{E}_{loc}(\omega_i)|^4/|\mathbf{E}_0(\omega_i)|^4$.

Hence for calculation of an enhancement factor G^{SERS}, taking into account the electromagnetic and geometric enhancement, the fourth power of the E-field amplitude is integrated across the surface and normalized by the area of a corresponding unstructured surface.

$$G^{\mathrm{SERS}} = \frac{1}{A_0}\int \frac{|E_{loc}|^4}{|E_0|^4}dA \tag{4}$$

This is an averaged enhancement factor assuming that the scattering molecules are distributed homogeneously across the substrate surface which is the case in many sensor applications.

The discretization is a crucial influencing factor for electromagnetic simulations of metallic structures. As the skin depth of electromagnetic radiation for gold lies in the range of 20-50nm for visible wavelengths the element size for the gold area is set to 5nm at maximum and to 1nm at maximum at the gold surface. With this resolution the exponential decay of the electromagnetic fields can be accurately resolved.

3 Results

3.1 Gratings

The geometry for rectangular gold coated gratings is illustrated in figure 1. A gold layer of constant thickness $t = 100$nm covers the periodically structured fused silica substrate. The corners of the structure are rounded with a radius of curvature of 1nm to achieve a more realistic model. The simulations are carried out for gratings with periods Λ between 100nm and 500nm as well as depths d between 25 and 200nm. For all gratings, the bumps and hollows are equally spaced with half the grating period.

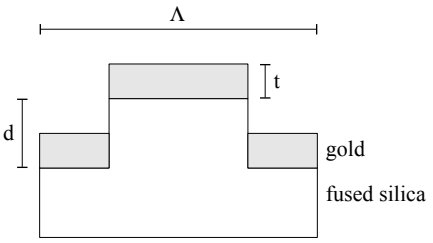

Figure 1: Model for a unit cell of the rectangular grating with period Λ, depth d and thickness t of the gold layer

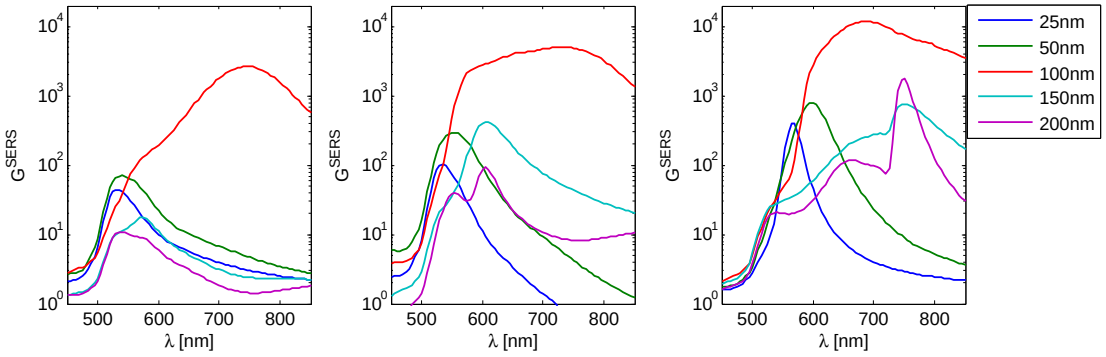

Figure 2: Modelled spectral Raman enhancement for a rectangular grating with period Λ=100nm (left), Λ=300nm (center), Λ=500nm (right) and varying depth between 25-200nm

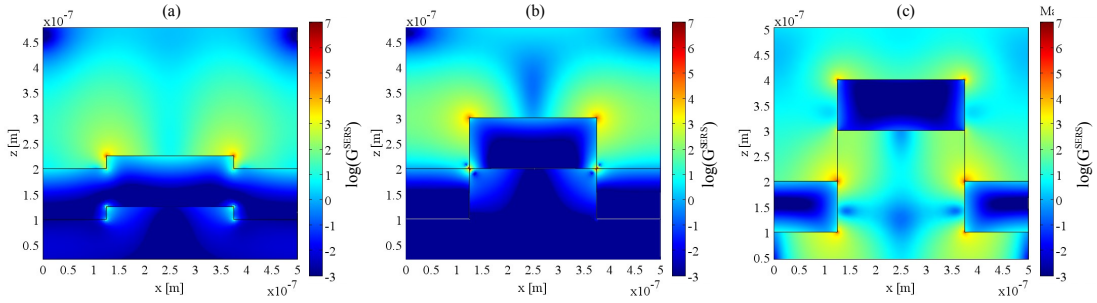

Figure 3: Logarithmic plot of Raman enhancement for a rectangular grating with period $\Lambda = 500$nm and (a) depth $d = 25$nm for an incident wavelength of $\lambda = 565$nm, (b) $d = 100$nm, $\lambda = 690$nm, (c) depth $d = 200$nm for an incident wavelength of $\lambda = 750$nm

Figure 2 shows the spectral Raman enhancement for different grating periods of 100nm, 300nm, 500nm from left to right. The enhancement factors strongly depend on the incident wavelength for a given geometry. This is due to the dispersion properties of plasmons which depend on size and shape of the metal nanostructures. For wavelengths smaller than the plasmon resonance wavelength of 510nm for very small gold particles plasmons cannot be excited and the enhancement is at most one order of magnitude. However, for wavelengths beyond 510nm the enhancements reach up to 4 orders of magnitude.

The largest enhancements are achieved for a grating depth of 100nm which corresponds to the gold layer thickness. For these gratings the enhancements at wavelengths beyond 600nm are between 3 and 4 orders of magnitude. A comparison of the enhancement factors for different grating periods of constant depth shows that the wavelength of the maximum enhancement is redshifted with increasing period. This is consistent with the plasmon resonance redshift of single metal nanoparticles which can be calculated using Mie theory. Furthermore, for depths beyond 100nm there arise two local maxima which is probably due to the spatial separation of the gold layer for these depths.

The evaluation of the Raman enhancement for constant grating periods shows that the wavelength of the maximum enhancement increases with depth – except for the depth of 100nm for small grating periods. Figure 3 shows a logarithmic plot of the local Raman enhancement factor for a grating with period Λ =500nm and increasing depth at the wavelength of maximum Raman enhancement, respectively. This wavelength increases from 565nm at a depth of 25nm to 750nm at a depth of 200nm. The maximum local enhancements are achieved at the corners of the metallic structure. This is due to the lightning rod effect arising at features with small radii of curvature in addition to the plasmon excitation of the whole metallic structure. The highest averaged enhancements are achieved at a depth of 100nm (also compare figure 2 (right)). This structure can be interpreted as closely arranged metallic cuboids which provide high enhancement at the points of closest approach additionally to the upper corners of the structure.

Figure 4 shows the Raman enhancement at a constant incident wavelength of 785nm for varying grating depth and different periods. For depths up to 100nm the enhancement is increasing with depth relatively independent on the period while for depths beyond 100nm it decreases monotonically. Moreover, for these larger depths the enhancement increases with period. Surprisingly the smaller structures do not necessarily show the higher enhancement factors. The optimal structure size depends on the geometry and the incident wavelength. Except for the depth of 100nm which shows extraordinary characteristics the optimal feature size increases with the incident wavelength.

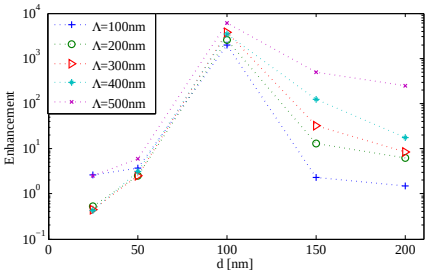

Figure 4: Relationship between Raman enhancement at a wavelength of 785nm for gratings with varying period Λ and grating depth

3.2 Spheres

Spherical metallic nanoparticles are common geometries for SERS applications. They can be produced by different procedures such as chemical or lithographical techniques or by laser ablation.

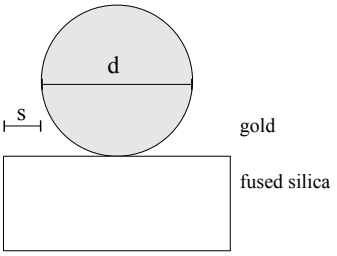

Figure 5: Model for a unit cell of the SERS surface consisting of spherical particles.

The geometry for the spherical particles is shown in figure 5. Gold particles of diameter d and separation s are placed on a fused silica substrate. The simulations cover particle sizes between 25nm and 500nm while the separation is varied in the range of 1-100nm.

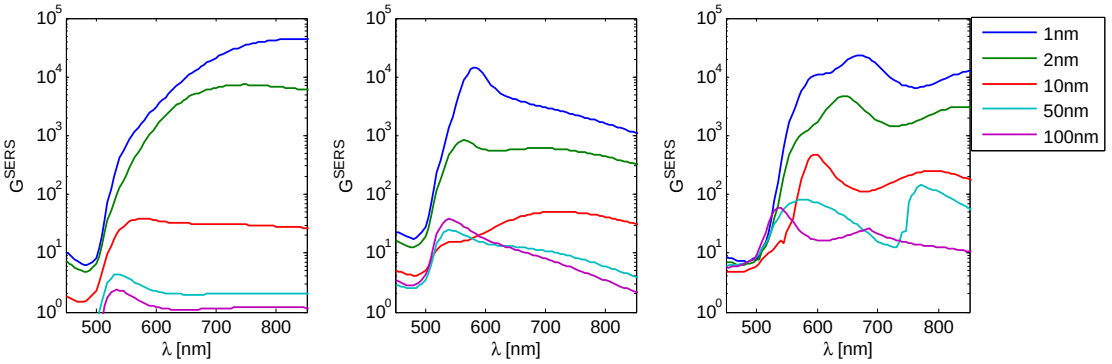

Figure 6: Modelled Raman enhancement for spheres with diameter $d = 25$nm (left), $d = 100$nm (center) and $d = 500$nm (right) for different particle separations between 1-100nm.

Figure 6 shows the spectral dependence of the Raman enhancement for different particle sizes and separations. In general, the enhancement is about one order of magnitude higher than for rectangular gratings. The wavelength of maximum enhancement is blueshifted with increasing particle separation. This is most obvious for particle sizes of 25nm (left) and 100nm (right) while the largest particles with a diameter of 500nm show multiple local maxima according to multipole resonances of higher orders which can be excited in large particles. Similarly to the grating structures, for wavelengths below 510nm the enhancement is small as no particle plasmons are excited. This is illustrated in figure 7. The logarithmic plot of the local Raman enhancement for spheres of diameter 500nm only shows small enhancement for an incident wavelength of 450nm (figure 7(a)). At a wavelength of 670nm (figure 7(b)) plasmons are excited resulting in high near fields and thus large enhancement.

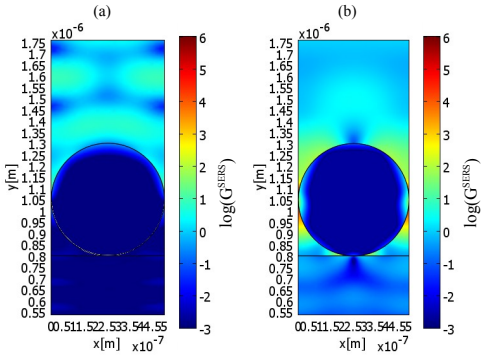

Figure 7: Logarithmic plot of Raman enhancement for spheres with diameter $d = 500$nm and separation s=1nm for an incident wavelength of (a) $\lambda = 450$nm, (b) $\lambda = 670$nm

Furthermore, a principal trend is the strong dependence of the predicted Raman enhancement on feature separation. For the spherical particles with a diameter of $d = 25$nm the difference between the enhancement for a separation of 1nm and 100nm is as large as 4 orders of magnitude. Figure 8 illustrates this dependence of the Raman enhancement on feature separation for different particle sizes for an incident wavelength of 785nm. It is evident that this relationship is relatively insensitive to feature size. For a small separation of 1nm the smallest spheres of diameter 25nm show the largest enhancement. However, with increasing feature separation this relationship is reversed.

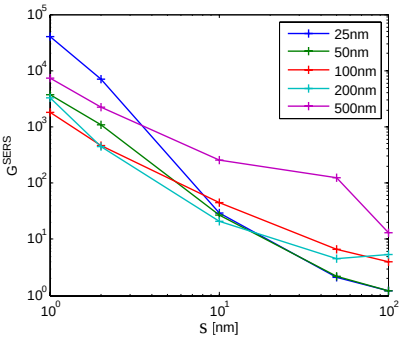

Figure 8: Relationship between Raman enhancement for spheres for an incident wavelength of $\lambda = 785$nm and feature separation for different particle diameters $d = 25 - 500$nm

For a separation of 100nm the enhancement increases monotonically with feature size, thus the largest spheres show maximum enhancement.

The enhancement factors of about 4 orders of magnitude for small feature separations agree quite well with Raman measurements carried out with thiophenol as Raman scattering substance. For a substrate covered with such gold nanoparticles the measured enhancement factors are about 10^6. Assuming that the chemical enhancement factor, which is not taken into account here, is about two orders of magnitude [5], the measured Raman enhancement is 10^4 and thus agrees with the simulations within one order of magnitude.

3.3 Hemispheres

Hemispherical metallic nanoparticles can be generated by similar techniques as spheres by using adhesive substrates. The geometry for a unit cell with hemispherical gold particles is illustrated in figure 9. The modelled sizes and separations are the same as for spherical particles.

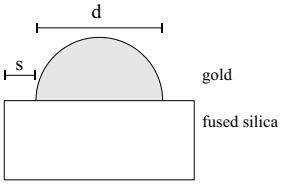

Figure 9: Model for a unit cell of the SERS surface consisting of hemispherical particles

Figure 11 shows the spectral dependence of the Raman enhancement for different particle sizes and separations. In general, the enhancements observed are 1-2 orders of magnitude higher than those for the spherical particles especially for larger particle sizes.

For the particles with a diameter of 100nm the wavelength of maximum enhancement is blueshifted with increasing particle separation while for the other particle sizes there is no monotonous dependence between separation and wavelength of maximum enhancement. Large hemispheres with a diameter of 500nm (right) show multiple local maxima similar to those of the spherical particles dicussed before. As well as for the other structures, for wavelengths below 510nm the enhancement is small since no plasmon excitation occurs.

The Raman enhancement of hemispherical particles also shows a strong dependence on feature separation already discussed for spheres. Figure 10 illustrates this relationship for an incident wavelength of 785nm. The difference between the enhancement for a separation of 1nm and 100nm is about 3-4 orders of magnitude for all particle sizes. In contrast to spherical particles the largest hemispheres of 500nm diameter show maximum Raman enhancement at 785nm for all feature separations.

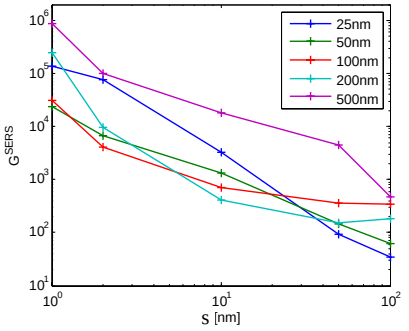

Figure 10: Relationship between enhancement for hemispheres for an incident wavelength of $\lambda = 785$nm and feature separation for different particle sizes of d =25-500nm

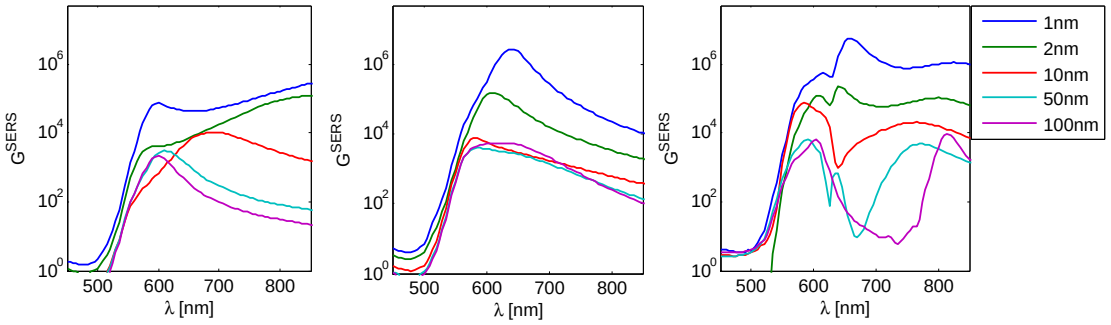

Figure 11: Modelled Raman enhancement for hemispheres with diameter d=100nm (left) d=100nm (center) and d=500nm (right) for particle separations between 1-100nm

4 Conclusion

The calculations yield several results: Firstly, there is a strong dependence on wavelength of the enhancement factors for a given geometry. This is due to the dispersion properties of plasmons which strongly depend on size and shape of the nanostructures. Secondly, small structures do not necessarily provide the largest enhancement. The grating with the largest period results in larger enhancement factors than the other gratings, especially for wavelengths beyond 600nm. Moreover, for spherical and hemispherical particles a small feature separation is crucial for high enhancements. The difference between Raman enhancements at 1nm and 100nm feature separation is as large as 3-4 orders of magnitude independent on particle size. Furthermore, hemispheres provide the largest Raman enhancement of all geometries analyzed here.

Although many influencing factors such as the exact position of the molecules at the surface and the influence of the chemical enhancement are not known in detail, Raman enhancements from metal nanoparticles on a fused silica substrate obtained experimentally agree with the simulations within one order of magnitude. The future aim will be to reliably predict SERS factors from a given substrate geometry and to be able to optimize the geometry of substrates with respect to their SERS enhancement.

References

[1] David P. Fromm, Arvind Sundaramurthy, Anika Kinkhabwala, P. James Schuck, Gordon S. Kino, and W. E. Moerner, *Exploring the chemical enhancement for surface-enhanced raman scattering with Au bowtie nanoantennas*, The Journal of Chemical Physics **124** (2006), no. 6, 061101.

[2] P. B. Johnson and R. W. Christy, *Optical constants of the noble metals*, Physical Review B **6** (1972), no. 12, 4370–4379.

[3] K. Kneipp, H. Kneipp, I. Itzkan, R R Dasari, and Michael S Feld, *Surface-enhanced raman scattering and biophysics*, Journal of Physics: Condensed Matter **14** (2002), R597–R624.

[4] Martin Moskovits, *Surface-enhanced spectroscopy*, Rev. Mod. Phys. **57** (1985), no. 3, 783–826.

[5] A. Otto, *Surface-enhanced raman scattering of adsorbates*, Journal of Raman Spectroscopy **22** (1991), 743–752.

[6] E. C. Le Ru, M. Meyer, E. Blackie, and P. G. Etchegoin, *Advanced aspects of electromagnetic SERS enhancement factors at a hot spot*, Journal of Raman Spectroscopy **39** (2008), 1127–1134.